Journal of Power Sources 254 (2014) 73–79

Contents lists available at ScienceDirect

Journal of Power Sources

journal homepage: www.elsevier.com/locate/jpowsour

Non-crystalline oligopyrene as a cathode material with a high-voltage plateau for sodium ion batteries

Su Cheol Han [1], Eun Gyoung Bae [1], Heatsal Lim, Myoungho Pyo*

Department of Printed Electronics Engineering, Sunchon National University, Sunchon, Chonnam 540-742, Republic of Korea

HIGHLIGHTS

- Oligopyrene (OPr) is used as a cathode in sodium ion batteries.
- Crystalline OPr shows large overpotentials with a down-sloping discharge curve.
- In contrast, amorphous OPr shows a voltage plateau at 3.5 V during discharge.
- The initial discharge capacity of 121 mAh g^{-1} is obtained.
- As a result, amorphous OPr shows a high-energy density of 423 Wh kg^{-1}.

ARTICLE INFO

Article history:
Received 22 November 2013
Received in revised form
20 December 2013
Accepted 21 December 2013
Available online 3 January 2014

Keywords:
Pyrene
Oligomer
Cathode
Energy density
Sodium ion batteries

ABSTRACT

Oligopyrene (OPr, 3–4 pyrene units) is chemically synthesized and used as a high-voltage organic cathode for sodium ion batteries (SIBs). OPr shows anion-dominant transport behaviors during redox-switching in $NaClO_4$ electrolytes, indicating that, when implemented in SIBs, OPr can reversibly incorporate/release perchlorate anions for charge-balance. A composite film, in which OPr maintains a crystalline phase with a layered structure, shows a sloping charge–discharge (C–D) curve (discharge capacity = 42.5 mAh g^{-1} and average voltage = 2.9 V vs. Na/Na^+ at 20 mA g^{-1}), implying a large overpotential due to slow ClO_4^- diffusion through the crystalline phase. In contrast, a composite film containing amorphous OPr exhibits substantially reduced overpotential with a plateau potential at 3.5 V during discharge. An initial reversible capacity of 121.0 mAh g^{-1}, which is close to one-electron transfer per pyrene unit, is decreased to 95.8 mAh g^{-1} during the first 10 C–D cycles, but is subsequently stabilized with a decreasing rate of 0.30 mAh g^{-1} per C–D cycle. The energy density of amorphous OPr (423 Wh kg^{-1} for the 1st discharge) is so large that it exceeds those of most inorganic-based cathode materials that have been reported thus far.

1. Introduction

Sodium ion batteries (SIBs) are at the fore in the field of new secondary ion battery research [1,2]. The development of alternatives to lithium ion batteries (LIBs), which was initially motivated by a deficiency of lithium reserves, is drawing more attention with the conceptual introduction of the smart grid system [3]. To realize electricity load leveling for a widespread smart-grid social network, which stores energy generated from intermittent power sources and manages energy consumption efficiently through communication with individual needs, the development of large-scale energy storage systems (ESS) at low cost is crucial [4]. The extensive use of LIBs for ESS in the smart-grid networks is doubtful due to both cost-effectiveness and safety concerns. In this regard, SIBs could be a viable alternative mainly because sodium is one of the most abundant elements on earth, which helps mitigate the concerns over the rising cost of mass consumption. The slightly higher standard reduction potential of a Na/Na^+ couple compared with a Li/Li^+ couple (0.305 V) could also be an additional benefit because it alleviates some safety concerns.

The fundamental chemistry behind the operation of SIBs is identical to that of LIBs, in that Na^+ ions released from the anode are inserted into the cathode during discharge and vice-versa during charge. From a material point of view, however, the ionic size of Na^+ is 1.3 times larger than that of Li^+, requiring the design of new electrode materials that can accommodate/release Na^+ without a severe energy barrier during transport. With respect to cathode materials, sodium transition metal oxides with layered

* Corresponding author. Tel.: +82 61 750 3638; fax: +82 61 750 3608.
E-mail address: mho@sunchon.ac.kr (M. Pyo).
[1] These authors contributed equally to this work.

0378-7753/$ – see front matter © 2013 Elsevier B.V. All rights reserved.
http://dx.doi.org/10.1016/j.jpowsour.2013.12.104

structures ($Na_xM^1_yM^2_zM^3_{1-y-z}O_2$) [5–10] and sodium transition metal phosphates of olivine ($NaM^1_xM^2_{1-x}PO_4$) [11–13] or NASICON ($Na_2M^1_xM^2_{2-x}(PO_4)_3$) [14–17] structures are representative examples for this purpose. Except few examples such as $NaFe_{0.5}Co_{0.5}O_2$ addressed by Komaba et al. [10], most of these cathode materials have shown a reversible Na^+ intercalation/deintercalation and are known to possess an initial capacity range of 80–100 mAh g^{-1}. Multi-step phase transitions ascribed to the insertion of large Na^+ ions into a solid state, however, can lead to severe decay in reversible capacities, which complicates the use of these materials for commercially viable cathodes in SIBs [18]. For example, P2-type Na_xCoO_2 experiences successive phase transitions through both single-phase and two-phase domains on sodium intercalations between $x = 0.5$ and 0.9 (i.e., stepwise voltage drop during discharge), requiring the suppression of phase changes in order to function as a reliable high-energy density cathode [19].

Since the phase transition of inorganic crystalline materials with sodium intercalation is a rather intrinsic property, the suppression of the phase changes is not easily attainable. In this regard, it makes sense to investigate organic materials as cathodes in SIBs. Recently, Okada et al. reported that disodium rhodizonate ($Na_2C_6O_6$), which was originally used for sustainable LIBs [20], shows a 2 Na^+ insertion equivalent per molecule (270 mAh g^{-1}) at between 1.0 and 2.9 V [21]. This cathode maintained reasonably good rate performance, but a discharge-first nature and a relatively low discharge voltage require further improvements for commercial viability. π-conjugated polymers (πCPs) [22,23], utilizing their p-doping/dedoping properties, were also being examined as cathodes for SIBs. Yang et al. claimed that ferrocyanide-incorporated polypyrrole matrix could be active for Na^+ insertion/desertion [22]. A high rate capability and a discharge capacity of more than 100 mAh g^{-1} at 200 mA g^{-1} have been reported. The discharge profiles, however, were rather capacitive-like, requiring further improvement to increase the energy density.

In the present study, we show that oligopyrene (OPr), as a representative example of polycyclic aromatic hydrocarbons (PAH) can be useful as a cathode of high-energy density in SIBs. PAH can demonstrate a high-voltage redox process, because the highest occupied molecular orbital (HOMO) level is sufficiently low (but higher than the energy level for electrolyte oxidation) due to aromaticity [24]. In a polymer composed of PAH units, the conjugation length is limited due to the geometric restrictions (i.e., orthogonality between PAH rings) [25]. Therefore, the effect of conjugation on the increase of a HOMO level becomes limited, conferring a high redox potential to the polymer. This characteristic contrasts with the behaviors of conventional πCPs such as polypyrrole [26] and polythiophene [27]. In πCPs, the extensive conjugation through main chains substantially raises the HOMO level of polymers so that πCPs of low redox potential become more suitable for electrode materials in aqueous electrolyte systems [28–30].

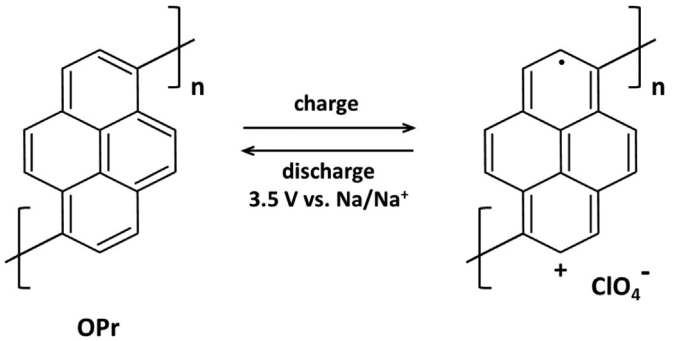

Scheme 1. Reversible charge–discharge process of oligopyrene, accompanying anion movement.

OPr is synthesized via interfacial polymerization and is utilized as a high-voltage cathode material in SIBs. Here, we use OPr rather than pyrene monomers not only because pyrene is dissolved in commonly used carbonate electrolytes, but also because the oxidation of pyrene during the first charge can release gaseous byproducts. For a half cell, while Na^+ is reduced on a Na metal during charge, OPr is oxidized with the incorporation of anions. This process occurs reversibly, showing a plateau voltage at 3.5 V (vs. Na/Na^+) with a large capacity (121.0 mAh g^{-1}) during discharge for amorphous OPr. The molecular structure and electrochemical reversibility of amorphous OPr are depicted in Scheme 1.

2. Experimental

OPr was synthesized at the interface between an *n*-hexane (150 mL) solution containing pyrene (20 mmol) and a nitromethane (100 mL) solution containing $FeCl_3$ (0.1 mol) at 50 °C for 24 h. It was addressed that the oxidation of pyrene by $FeCl_3$ produces linear OPr chains through 1,1′ (or 2,2′) coupling [31] rather than polypyrene dendrimers [25]. The OPr precipitate was collected by centrifugation and washed with n-hexane and ethanol repeatedly. A greenish yellow powder was obtained after vacuum drying.

The molecular weight of OPr was determined via matrix-assisted laser desorption/ionization-time of flight mass spectrometry (MALDI-TOF MS, Applied Biosystems, VOYAGER STR), employing 2,5-dihydroxybenzoic acid as the matrix and a 337 nm N_2 laser (3 ns pulse) for excitation. UV–Vis (JASCO, V-670) and fluorescence spectra (SLM AMINCO) were recorded to further confirm the oxidative oligomerization of pyrene. The mass changes of the OPr film, which was electrochemically deposited on Au-coated AT-cut quartz crystal, were monitored during redox-switching using an electrochemical quartz crystal nanobalance (EQCN, SEIKO EG&G, QCA922, resonance frequency = 9 MHz). The retention of the crystallinity of the OPr after the construction of the composite films was confirmed by X-ray diffraction (XRD) using a Rigaku ULTIMA 4 equipped with Cu K_α radiation at a scan rate of 2° min^{-1}. Morphological and particle size characterizations were carried out using a Hitachi S3500 field emission scanning electron microscope (FESEM).

The coin cells (CR 2032) of a Na/electrolyte/OPr configuration, in which the glass filter was sandwiched between 2 electrodes, were assembled in an Ar-filled glove box (O_2, $H_2O < 1$ ppm). The OPr electrode was a mixture of 80% OPr, 10% acetylene black (AB), and 10% poly(vinylidene fluoride) (PVdF). To make amorphous OPr, a solvent common to both OPr and PVdF (*N*-methylpyrrolidone, NMP) was used during the slurry preparation. Crystalline OPr, on the other hand, was prepared in a nonsolvent for OPr (diethylene glycol monoethyl ether acetate, DGA) to maintain the crystalline nature of as-synthesized OPr. OPr-coated Al foils were punched to form a disk with a diameter of 1.6 cm that was then welded to a stainless steel case [32]. The $NaClO_4$ was dissolved in propylene carbonate to be a concentration of 1.0 M. A galvanostatic charge–discharge cycle test was performed using an automatic WBCS 3000 battery cycler (WonATech) in a potential range of 2.0–4.5 V vs. Na/Na^+. All assembled cells were stored for at least 1 h at room temperature before testing. For electrochemical impedance spectroscopy (EIS) measurements, a Princeton Applied Research PARSTAT 2273 potentiostat was used and measurements were conducted by applying a 10 mV AC signal at 2.5 and 3.5 V vs. Na/Na^+ over the frequency range of $10^{-1} - 10^5$ Hz. The obtained EIS was analyzed using Z-View software (Scribner and Associates Inc.).

3. Results and discussion

3.1. Ion transport behaviors of OPr thin film

OPr thin film was potentiostatically synthesized on Au-coated quartz at 1.2 V (vs. Ag/AgCl) until the charge passage and the frequency change reached 6.1 mC cm^{-2} and 2000 Hz (mass change = 11.2 μg cm^{-2}), respectively. To confirm the ion transport behaviors of OPr, the thin film was redox-cycled in a pyrene-free acetonitrile solution of 0.1 M $NaClO_4$ by EQCN. The current and mass changes of OPr during potential cycling at 50 mV s^{-1} are shown in Fig. 1. The voltammogram indicates that the OPr can be reversibly redox-switched at an $E_{1/2}$ of ca. 0.91 V (3.81 V vs. Na/Na^+). A concurrent mass increase and decrease with oxidation and reduction of OPr were also obvious, indicating the anion-dominant ion transport behaviors [33].

Because the oxidation of pyrene at 1.0 V accompanied the oxidation (p-doping) of deposited OPr, the charge (6.0 mC cm^{-2}) and mass (11.2 μg cm^{-2}) during film deposition also included the responses from the charge consumed for OPr oxidation and the mass increase due to the influx of counter anions (ClO_4^-), respectively. Therefore, a comparison of these values with the passed charge (2.5 mC cm^{-2}) and the mass increase (4.1 μg cm^{-2}) during OPr redox, which is shown in Fig. 1, provided the doping level of OPr. Assuming that pyrene units were oligomerized through 1–1′ linkage [31], it can be inferred that a one-electron transfer and a one-anion movement (ClO_4^-) per pyrene unit occurred during OPr redox, signifying that the OPr could possess a reversible capacity of 134 mAh g^{-1} (theoretical capacity) when used as a cathode in SIBs.

3.2. Chemical synthesis of OPr

The degree of oxidative polymerization of pyrene was confirmed by MALDI-TOF MS. The characteristic signals of the matrix were subtracted from the spectrum. The top panel of Fig. 2 shows one dominant signal at a mass/charge (m/z) of 602.9, which coincides with the molecular weight of three pyrene units. The additional peak located at an m/z of 801.9 also corresponds to the molecular weight of pyrene tetramers. Thus, the MS spectrum indicates that the polymerization was limited to oligomer formations of 3 or 4 pyrene units due to the steric restriction between planar PAH rings. Considering the reasons for performing polymerization (i.e., prevention of the oxidative polymerization of pyrene during the charge and dissolution of pyrene monomers into carbonate electrolytes by using the polymer rather than the monomer as a cathode active material), the formation of an oligomer is rather beneficial. This is because the redox potential of the pyrene-based cathode could be substantially decreased in a high molecular weight polymer, although to some extent the orthogonality between PAH rings hampers the extensive π-conjugation.

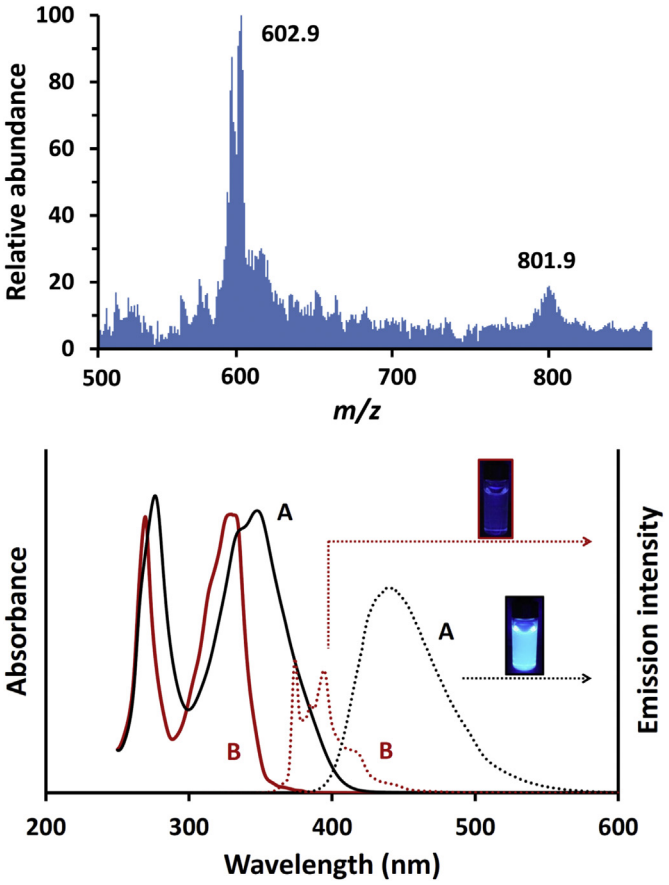

Fig. 2. (top) MALDI-TOF MS spectrum of chemically synthesized OPr. (bottom) UV–Vis absorbance and fluorescence spectra of (A) OPr and (B) pyrene, dissolved in NMP to be 0.1 mM.

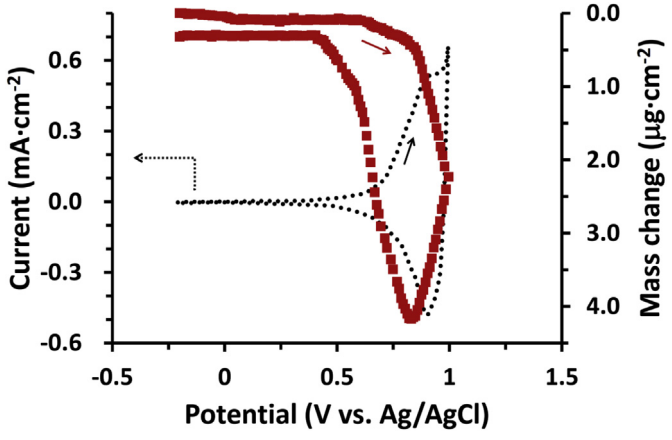

Fig. 1. (dotted line) Current and (square mark) mass changes during redox-switch of OPr in an acetonitrile solution of 0.1 M $NaClO_4$ at 50 mV s^{-1}.

To further confirm the oligomerization, the UV–Vis absorption and fluorescence spectra of pyrene and OPr were compared. The bottom panel of Fig. 2 demonstrates that the onset of UV absorption was observed at 410 nm for OPr (A), which was ca. 50 nm longer than the onset of pyrene (B). The reduction of a π–π* bandgap of as much as 0.42 eV (corresponding to 50 nm onset shift) after oligomerization implies that the overlap of the p-orbitals between the PAH rings was not completely prohibited. The OPr also emitted more intense fluorescence at a longer wavelength compared with a monomer at the same concentration (0.1 mM) in NMP, once again indicating a partial π-conjugation throughout the entire OPr molecule.

The crystalline natures of pyrene monomers and OPr were compared using XRD (Fig. 3). The diffractogram of pyrene corresponded to the crystallographic structure of monoclinic $P2_1/a$ (JCPDS No. 025–1938) with the strongest peak at 10.52° in 2θ [34]. Once it was polymerized, the diffraction pattern of OPr was changed completely. A series of well-developed diffraction peaks at 11.10°, 16.32°, and 22.98° in 2θ, which corresponded to d-spacing of 0.80, 0.54, and 0.39 nm, respectively, were evident. These features agreed well with that of electrochemically polymerized OPr, indicating that OPr possessed a layered structure with interlayer spacing (d_{100}) of 1.6 nm [34,35].

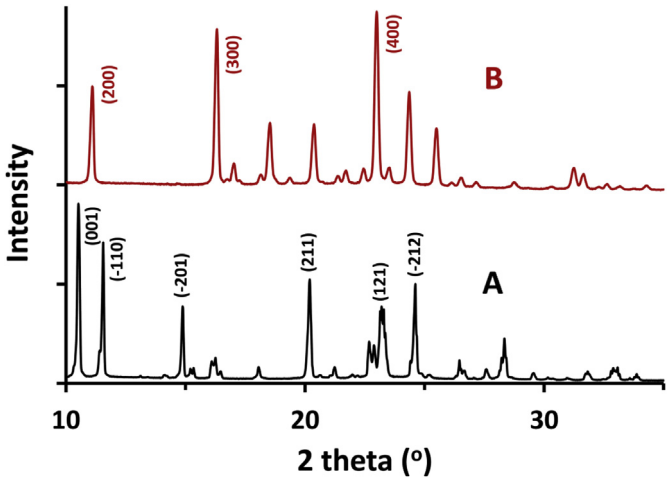

Fig. 3. XRD patterns of (A) pyrene monomers and (B) OPr.

3.3. Electrochemical properties of crystalline OPr

To confirm the electrochemical performance of the crystalline OPr, a composite film was prepared in DGA. OPr was insoluble in DGA, but PVdF was soluble. The XRD patterns of the composite film shown in Fig. 4A clearly demonstrate that the crystalline property of OPr was retained when the composite was prepared in DGA (Although a perfect pattern-match with the diffractogram of OPr powder was not the case, major diffraction peaks indicating a layered structure were invariant.).

The C–D profiles of crystalline OPr, recorded at 20 mA g^{-1} (0.15 C-rate), are shown in Fig. 4B. It is obvious that the discharge capacity was relatively small at ca. 42.5 mAh g^{-1} during the 1st discharge. The voltage continuously decreased with an average of ca. 2.9 V, indicating that the crystalline OPr possessed an energy density of 123 Wh kg^{-1}, which is far below that of $NaFe_{0.5}Co_{0.5}O_2$ [10], but similar to that of most inorganic-based cathodes [2]. As implied in the inset of Fig. 4B, the low-energy density of crystalline OPr resulted mainly from a large degree of polarization. Note that a voltage hysteresis of as much as 1.3 V between charge and discharge segments was abnormally large. The cyclability of crystalline OPr was also unsatisfactory, as shown in Fig. 5. The 1st discharge capacity of 42.6 mAh g^{-1} was increased slightly to 45.0 mAh g^{-1} at the 3rd discharge, but was decreased with cycling from the 4th cycle to reach 27.4 mAh g^{-1} at the 50th cycle. The coulombic efficiency was also low, showing less than 98.5% for all cycles. The low coulombic efficiency, during the initial few cycles in particular, is likely related to the interfacial reaction on the OPr surface, which becomes pronounced due to low discharge capacities.

3.4. Amorphous OPr with high-energy density

Since we speculated that the low electronic conductivity of OPr (10^{-8} S cm^{-1} in a virgin state and 10^{-3}–10^{-5} S cm^{-1} in a doped state) [31,34,35] and/or the sluggish diffusion of anions through molecular-level stacks would induce a large polarization in crystalline OPr, a composite film containing amorphous OPr was prepared in OPr-soluble solvent (NMP). As expected, OPr dissolved in NMP together with PVdF was not crystallized during NMP evaporation. Fig. 6A shows the XRD patterns of a composite film prepared in NMP. In contrast with a composite film made in DGA, no sharp diffraction lines were seen, indicating that most of the OPr was in an amorphous state. The FESEM images of the composite films showed that, while a composite film prepared in DGA contained distinct OPr crystalline particles, a composite film prepared in NMP possessed no OPr particles, but instead consisted of the AB particles that seemed well connected by the polymer (OPr and PVdF) (Fig. 6B). Therefore, it is believed that OPr covers AB particles as a thin layer, which is expected to significantly reduce the voltage-loss ascribed to overpotentials.

The C–D behaviors of amorphous OPr were distinctively different from those of crystalline OPr. As shown in Fig. 7, the amorphous OPr delivered a reversible capacity that was three times

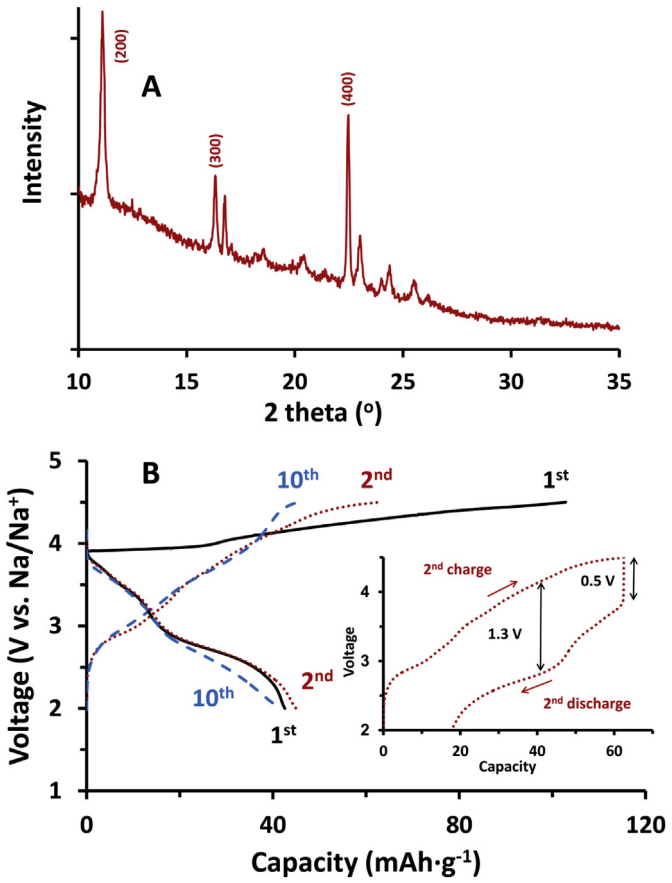

Fig. 4. (A) XRD patterns and (B) C–D profiles of crystalline OPr. Inset shows the 2nd C–D profile to indicate a large overpotential. Current density = 20 mA g^{-1}.

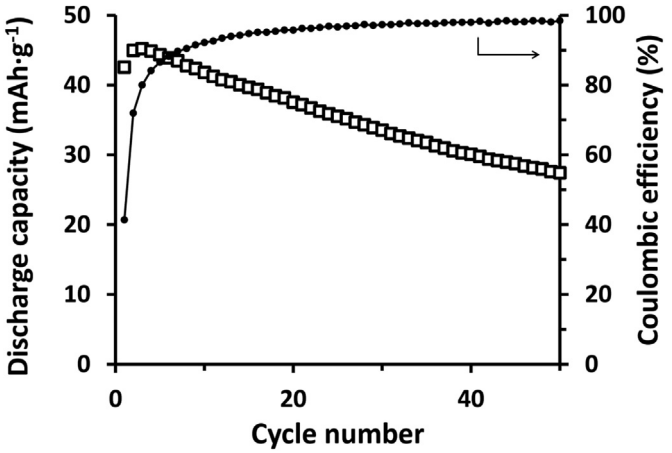

Fig. 5. Retention of discharge capacities and coulombic efficiency of crystalline OPr.

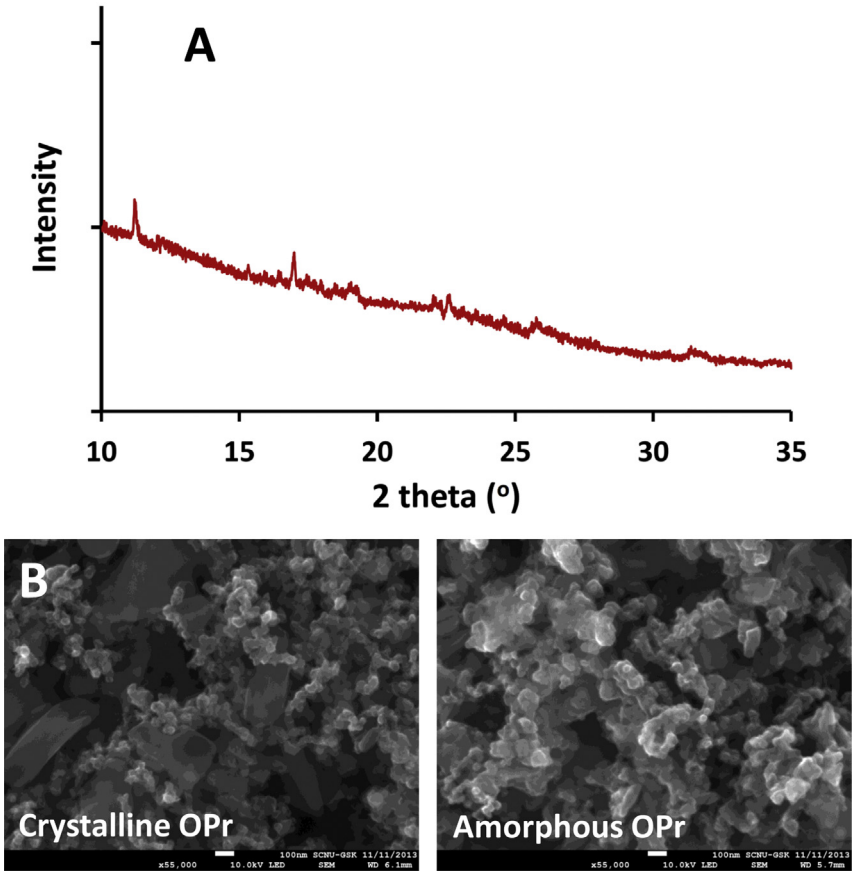

Fig. 6. (A) XRD patterns and (B) FESEM images of amorphous OPr. For comparison, FESEM image of crystalline OPr is also included.

greater than that of crystalline OPr. The discharge capacity of the former was ca. 120 mAh g^{-1} during the initial few cycles, compared with a discharge capacity of 42.5 mAh g^{-1} during the 1st cycle for the latter. The high capacity of amorphous OPr is either comparable [10] or superior [2,36] to most inorganic materials containing transition metals. Moreover, the C–D process of amorphous OPr proceeded in a narrow voltage range, showing charge and discharge plateaus. The dQ/dV curves in the inset of Fig. 7 more clearly show that the charge and discharge processes occurred at 3.78 and 3.54 V (peak separation of 0.24 V and $E_{1/2}$ of 3.66 V) and that this redox pair was responsible for the largest fraction of the total capacity. The sharp peak at 4.06 V and the small hump at 4.34 V that appeared during the 2nd charge were gradually weakened with cycling, resulting in complete disappearance at the 10th charge. The combination of a high-voltage plateau (ca. 3.5 V) and a great capacity (ca. 120 mAh g^{-1}) accounts for the unprecedented high-energy density of the amorphous OPr (423 Wh kg^{-1}).

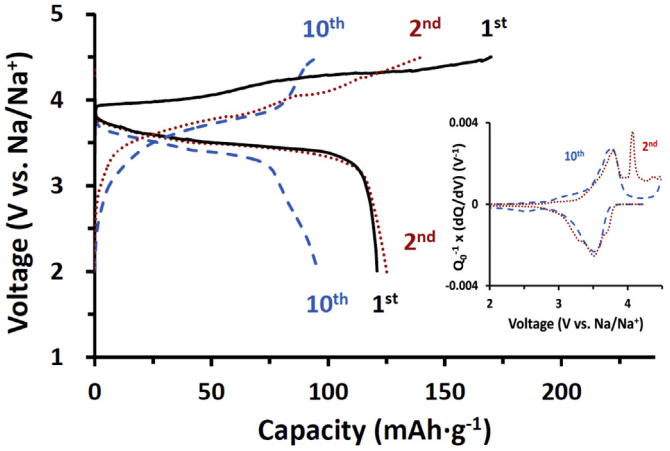

Fig. 7. C–D profiles of amorphous OPr at a current density of 20 mA g^{-1}. Inset shows dQ/dV curves for the 2nd and 10th cycles.

The inset of Fig. 7 also shows that, while the oxidation peaks above 4 V disappeared with cycling, the peak position and height of a reversible redox pair located at 3.66 V remained constant. Note that charge capacities of up to 4.0 V for the 2nd and 10th cycles were similar at ca. 70 mAh g^{-1} (Fig. 7). This invariance was interesting because it suggested the minimal capacity that was obtainable after prolonged cycling. Fig. 8A shows that the discharge capacity was decreased rapidly with cycling during the initial 10 cycles (from 121.0 mAh g^{-1} to 95.8 mAh g^{-1}), but was stabilized at a decreasing rate of 0.30 mAh g^{-1} for subsequent C–D cycles. The coulombic efficiency also reached more than 99% after 10 C–D cycles.

The rate performance of amorphous OPr was also investigated. Fig. 8B shows a stepwise decrease in the discharge capacity with an increase in current densities from 20 (0.15 C) to 500 mA g^{-1} (3.7 C). The capacities were recorded after the C–D curves had reached a stationary state (i.e., after 10 C–D cycles at 20 mA g^{-1}). Although the capacity dropped to ca. 10 mAh g^{-1} at 500 mA g^{-1}, the amorphous OPr still delivered a capacity of ca. 60 mAh g^{-1} at 100 mA g^{-1} (0.75 C). When returned to 20 mA g^{-1}, the amorphous OPr showed an immediate recovery of the initial capacity.

Finally, EIS spectra were obtained to compare the charge transfer and diffusion kinetics between crystalline and amorphous OPr at 2.5 and 3.5 V (Fig. 9). Since OPr is in an insulating state at 2.5 V, both materials showed two depressed semicircles (including one incomplete semicircle). Since two mobile charge

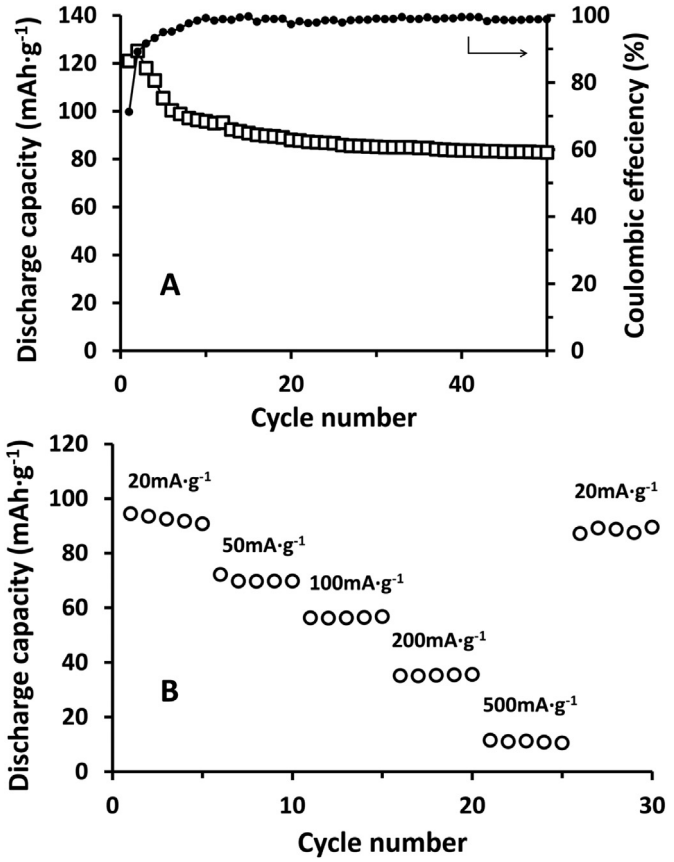

Fig. 8. (A) Retention of discharge capacities and coulombic efficiency and (B) rate performance of amorphous OPr. The numbers indicate current densities in mA g^{-1}.

carriers (electrons and anions) can contribute to the impedance behaviors, a complete semicircle at high frequencies and an incomplete semicircle at low frequencies appear to represent the impedance due to the charge transfer of electrons and anions, respectively [37]. It was obvious that at 2.5 V, the sum of charge transfer resistances (R_{ct}) was much greater in crystalline OPr than in amorphous OPr, although both materials were in an insulating state. When oxidized at 3.5 V, the charge transfer impedance was decreased significantly. The spectra appeared to consist of one semicircle at high frequencies and a Warburg-like straight line at low frequencies. The merging of two distinctive

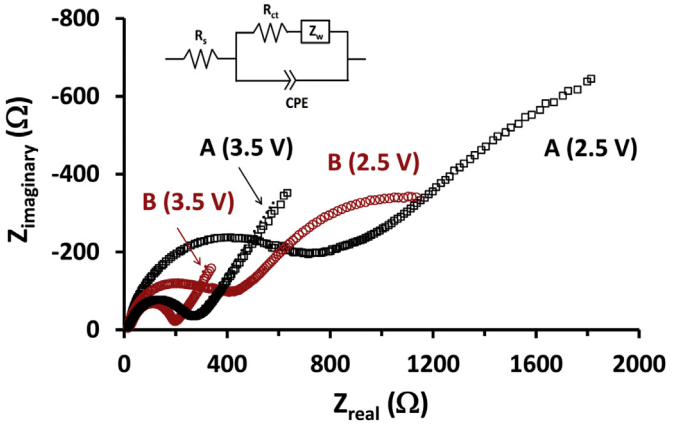

Fig. 9. EIS spectra of (A) crystalline and (B) amorphous OPr. Inset shows an equivalent circuit used to analyze spectra obtained at 3.5 V. R_s = solution resistance, R_{ct} = charge transfer resistance, CPE = constant phase element, and Z_w = Warburg impedance.

semicircles was believed due to a drastic increase in the electronic conductivity at the oxidized state of OPr. Utilizing the equivalent circuit shown in the inset of Fig. 9, the EIS spectra obtained at 3.5 V were analyzed and the electrochemical parameters were extracted. While a negligible difference in R_{ct} was confirmed (218 and 201 Ω for the crystalline and the amorphous, respectively) due to the enhanced conductivities at 3.5 V, there was a significant difference in the diffusion of ClO_4^- anions through the OPr. The diffusion coefficient was calculated using the following equation [38,39]

$$D = \left(\frac{RT}{\sqrt{2}AF^2\sigma C}\right)^2 \quad (1)$$

where D is the diffusion coefficient of chloride, $m^2\ s^{-1}$, R is the gas constant ($JK^{-1}\ mol^{-1}$), T is the temperature (K), A is the electrode area (m^2), F is the Faraday constant ($C\ mol^{-1}$), Ω is the Warburg prefactor ($\Omega\ s^{-1}$), and C is the concentration of ClO_4^- ($mol\ m^{-3}$). Using the Warburg prefactors of 22 and 356 $\Omega\ s^{-1}$, the diffusion coefficients of 7.0×10^{-18} and $1.7 \times 10^{-15}\ m^2\ s^{-1}$ were obtained for crystalline and amorphous OPr, respectively. More than two orders of magnitude difference in the diffusion coefficient suggests that thin films of the amorphous OPr coated on conducting additives facilitates anion diffusion, which contributes to a high plateau voltage and a great capacity of OPr. It is also worth mentioning that the solution resistance (R_s) was unchanged with oxidation states of OPr within an experimental error range. R_s values of 14.2 Ω at 2.5 V and 14.5 Ω at 3.5 V for amorphous OPr indicated that the decrease in ionic strength of electrolytes during charging did not affect cell performance.

4. Conclusions

In the present study, OPr, which shows anion-dominant transport behaviors during redox-switching in $NaClO_4$ electrolyte, is used as a high-voltage organic cathode for SIBs. OPr existing as crystalline phases in the composite film exhibits a down-sloping discharge curve (discharge capacity = 42.5 mAh g^{-1} and average voltage = 2.9 V vs. Na/Na^+ at 20 mA g^{-1}), due to the large overpotential ascribed to slow ClO_4^- diffusion through a crystalline phase. In contrast, OPr retaining an amorphous nature in a composite film exhibits a substantially reduced overpotential with a plateau voltage at 3.5 V during discharge. An initial reversible capacity of 121.0 mAh g^{-1} is decreased to 95.8 mAh g^{-1} during first 10 C–D cycles, but is subsequently stabilized with a decreasing rate of 0.30 mAh g^{-1} per C–D cycle. We believe that the energy density of amorphous OPr (423 Wh kg^{-1} for the 1st discharge) exceeds those of most cathode materials reported thus far, suggesting an alternative approach to the development of new cathode materials for SIBs.

Acknowledgments

This research was supported by the Basic Science Research Program through the National Research Foundation of Korea (NRF) funded by the Korea Government (MSIP) (No. 2013R1A2A2A04015089). The authors also appreciate the scholarship fund by Brain Korea 21 Plus ($BK21^+$).

References

[1] B.L. Ellis, L.F. Nazar, Curr. Opin. Solid State Mat. Sci. 16 (2012) 168–177.
[2] S.-W. Kim, D.-H. Seo, X. Ma, G. Cedar, K. Kang, Adv. Energy Mater. 2 (2012) 710–721.

[3] H. Lund, A.N. Andersen, P.A. Østergaard, B.V. Mathiesen, D. Connolly, Energy 42 (2012) 96–102.
[4] Z. Yang, J. Zhang, M.C.W. Kintner-Meyer, X. Lu, D. Choi, J.P. Lemmon, J. Liu, Chem. Rev. 111 (2011) 3577–3613.
[5] N. Yabuuchi, M. Yano, H. Yoshida, S. Kuze, S. Komaba, J. Electrochem. Soc. 160 (2013) A3131–A3137.
[6] J.J. Ding, Y.N. Zhou, Q. Sun, X.Q. Yu, X.Q. Yang, Z.W. Fu, Electrochim. Acta 87 (2013) 388–393.
[7] S. Komaba, N. Yabuuchi, T. Nakayama, A. Ogata, T. Ishikawa, I. Nakai, Inorg. Chem. 51 (2012) 6211–6220.
[8] N. Yabuuchi, M. Kajiyama, J. Iwatate, H. Nishikawa, S. Hitomi, R. Okuyama, R. Usui, Y. Yamada, S. Komaba, Nat. Mater. 11 (2012) 512–517.
[9] D. Carlier, J.H. Cheng, R. Berthelot, M. Guibnard, M. Yoncheva, R. Stoyanova, B.J. Hwang, C. Delmas, Dalton Trans. 40 (2011) 9306–9312.
[10] H. Yoshida, N. Yabuuchi, S. Komaba, Electrochem. Commun. 34 (2013) 60–63.
[11] K. Zaghib, J. Trottier, P. Hovington, F. Brochu, A. Guerfi, A. Mauger, C.M. Julien, J. Power Sources 196 (2011) 9612–9617.
[12] K.T. Lee, T.N. Ramesh, F. Nan, G. Botton, L.F. Nazar, Chem. Mater. 23 (2011) 3593–3600.
[13] P. Moreau, D. Guyomard, J. Gaubicher, F. Boucher, Chem. Mater. 22 (2010) 4126–4128.
[14] K. Chihara, A. Kitajou, I.D. Gocheva, S. Okada, J.-I. Yamaki, J. Power Sources 227 (2013) 80–85.
[15] L.S. Plashnitsa, E. Kobayashi, Y. Noguchi, S. Okada, J. Yamaki, J. Electrochem. Soc. 157 (2010) A536–A543.
[16] C. Demas, A. Nadiri, J.L. Soubeyroux, Solid State Ionics 28 (1988) 419–423.
[17] C. Delmas, F. Cherkaoui, A. Nadiri, P. Hagenmuller, Mater. Res. Bull. 22 (1987) 631–639.
[18] H. Wang, B. Yang, X.-Z. Liao, J. Xu, D. Yang, Y.-S. He, Z.-F. Ma, Electrochim. Acta 113 (2013) 200–204. http://dx.doi.org/doi:10.1016/j.electacta.2013.09.098.
[19] R. Berthelot, D. Carlier, C. Delmas, Nat. Mater. 10 (2011) 74–80.
[20] H. Chen, M. Armand, G. Demailly, F. Dolhem, P. Poizot, J.-M. Tarascon, ChemSusChem 1 (2008) 348–355.
[21] K. Chihara, N. Chujo, A. Kitajou, S. Okada, Electrochim. Acta 110 (2013) 240–246. http://dx.doi.org/doi:10.1016/j.electacta.2013.04.100.
[22] M. Zhou, L. Zhu, Y. Cao, R. Zhao, J. Qian, X. Ai, H. Yang, RSC Adv. 2 (2012) 5495–5498.
[23] R. Zhao, L. Zhu, Y. Cao, X. Ai, H.X. Yang, Electrochem. Commun. 21 (2012) 36–38.
[24] Y. Natsume, T. Minakata, T. Aoyagi, Thin Solid Films 517 (2009) 3005–3010.
[25] T.M. Figueira-Duarte, S.C. Simon, M. Wagner, S.I. Druzhinin, K.A. Zachariasse, K. Mullen, Angew. Chem. Int. Ed. 47 (2008) 10175–10178.
[26] M. Pyo, C.-H. Kwak, Synth. Met. 150 (2005) 133–137.
[27] V. Saji, K. Zong, M. Pyo, J. Photochem. Photobiol. A Chem. 212 (2010) 81–87.
[28] L. Liu, F. Tian, M. Zhou, H. Guo, X. Wang, Electrochim. Acta 70 (2012) 360–364.
[29] G. Wang, Q. Qu, B. Wang, Y. Shi, S. Tian, Y. Wu, Chem. Phys. Chem. 9 (2008) 2299–2301.
[30] H. Qin, Z.P. Song, H. Zhan, Y.H. Zhou, J. Power Sources 249 (2014) 367–372, http://dx.doi.org/10.1016/j.jpowsour.2013.10.091.
[31] X.-G. Li, Y.-W. Liu, M.-R. Huang, S. Peng, L.-Z. Gong, M. Moloney, Chem. Eur. J. 16 (2010) 4803–4813.
[32] S.J.R. Prabakar, Y.-H. Hwang, E.-G. Bae, S. Shim, D. Kim, M.S. Lah, K.-S. Sohn, M. Pyo, Adv. Mater. 25 (2013) 3307–3312.
[33] J.H. Hwang, M. Pyo, Synth. Met. 157 (2007) 155–159.
[34] L. Qu, G. Shi, Chem. Commun. (2004) 2800–2801.
[35] G. Lu, L. Qu, G. Shi, Electrochim. Acta 51 (2005) 340–346.
[36] J. Xu, D.H. Lee, Y.S. Meng, Func. Mater. Lett. 6 (2013) 13300011–13300017.
[37] M.D. Levi, D. Aurbach, J. Electrochem. Soc. 149 (2002) E215–E221.
[38] T. de J. Lincona-Sánchez, G.A. Álvarez-Romero, L.H. Mendoza-Huizar, C.A. Galán-Vidal, M. Palomar-Pardavé, M. Romero-Romo, H. Herrera-Hernández, J. Uruchurtu, J.M. Juárez-García, J. Phys. Chem. B 114 (2010) 9737–9743.
[39] R. Vedalakshmi, V. Saraswathy, H.-W. Song, N. Palaniswamy, Corr. Sci. 51 (2009) 1299–1307.